Japanese Journal of Applied Physics
Vol. 47, No. 6, 2008, pp. 5070–5075

Optical Heating of Ink-Jet Printable Ag and Ag–Cu Nanoparticles

Junggwon YUN, Kyoungah CHO, Byoungjun PARK, Ho Chul KANG[1], Byeong-Kwon JU, and Sangsig KIM*

Department of Electrical Engineering and Institute for Nano Science, Korea University, Seoul 136-701, Korea
[1]*LG Phillips LCD R&D Center, 533 Hogae-dong, Dongan-gu, Anyang, Kyeonggi-do 431-080, Korea*

(Received November 8, 2007; accepted April 7, 2008; published online June 20, 2008)

Ink-jet printable Ag nanoparticles (NPs) and Ag–Cu alloy NPs were synthesized by the polyol method, and interconnection lines composed of these NPs were fabricated on poly(ether sulfone) substrates. The effect of optical heating on the resistivity of the interconnections was investigated as functions of the irradiation time and power of the 488-nm wavelength light. The resistivities of the interconnection lines composed of the NPs were decreased by 7–10 times after the irradiation of the light with a power of 400 mW for 30 min, compared with the interconnection lines composed of the as-synthesized NPs. In addition, the change in the current of the interconnection line when the substrate is bent is discussed in this paper.
[DOI: 10.1143/JJAP.47.5070]

KEYWORDS: Ag, Ag–Cu, optical heating, ink-jet

1. Introduction

Recently, electrical circuits fabricated by the ink-jet printing of metal nanoparticle (NP) suspensions have been extensively investigated in the field of organic electronics, due to the applicability of ink-jet printing to a variety of substrates including plastic substrates.[1,2] Ink-jet printable metal NPs can be used as electrodes or interconnection lines after the enhancement of their electrical characteristics by thermal heating at temperatures higher than 200 °C; the thermal heating causes the metal NPs to be sintered and annealed, leading to the enhancement of their electrical properties.[3–5] Unfortunately, thermal heating may not be applicable to the fabrication of electrodes or interconnection lines made of metal NPs on top of plastic substrates, since it causes damage to the plastic substrates. Therefore, in order to utilize metal NP inks as interconnection materials in flexible electronics, alternative heating techniques are required to enhance the electrical conductivity of the metal NPs without damaging the plastic substrates. Recently, the optical heating of metal NPs has been developed as one of the alternative heating techniques.[6,7]

Among the variety of metal NPs, Ag NPs have been investigated as a candidate material for electrode or interconnection lines in flexible electronics, since Ag films have a lower resistivity (1.63 μΩ·cm) and melting point (961.8 °C) than other metal films. Nevertheless, pure Ag lines are liable to induce system failure resulting from the electromigration of ions, which is one of the main reliability issues in modern integrated circuits. It was reported in refs. 8 and 9 that the alloying of Cu into Ag reduces the electromigration. In this work, Ag and Ag–Cu NPs were synthesized by the polyol process, one of the typical methods of synthesizing metal NPs by chemical reduction.[10,11] Interconnection lines composed of Ag NPs or Ag–Cu alloy NPs fabricated on poly(ether sulfone) (PES) substrates were prepared, and their electrical characteristics were investigated with and without optical heating.

2. Experiments

Ag NPs and Ag–Cu NPs were synthesized by the polyol method.[12,13] 9 mg of poly(vinyl pyrrolidone) (PVP; MW 10,000, Aldrich) was dissolved in 50 ml ethylene glycol. This solution was stirred at 60 °C. After 0.3 g of silver nitrate (Aldrich) was added, the reaction was allowed to continue for 10 min. The color of the solution changed immediately from colorlessness to pale brown, indicating the synthesis of Ag NPs. Ag–Cu alloy NPs were also synthesized using a method similar to that used for the preparation of the Ag NPs. 3.987 g of PVP (MW 58,000, Aldrich) and 0.216 g of copper acetate hydrate (Aldrich) were dissolved in 30 ml of ethylene glycol. This solution was purged by nitrogen gas for 30 min and held at 175 °C for 20 min. Silver nitrate of 0.3337 g was then added to the solution and the reaction was allowed to continue for 10 min. After the metal NPs were synthesized, they were separated by centrifugation and washed with acetone and methanol several times to remove the PVP in the NP powder. The powders of synthesized metal NPs were dissolved in water, and the solution was dropped on a patterned PES substrate previously subjected to UV/ozone treatment to render its surface hydrophilic. The 488-nm wavelength light obtained from an Ar laser was used as a light source to heat the Ag NPs and the Ag–Cu alloy NPs.

The absorption spectra of the solutions containing the Ag NPs or the Ag–Cu alloy NPs were taken with a PGENRAL TU-1800 spectrophotometer. The structural properties of the metal NPs were characterized by X-ray diffraction (XRD; Philips Xpert System) and transmission electron microscopy (TEM; TECHNAI F30 G2). The thicknesses of the interconnection lines made of the NPs were measured by an alpha-step 500 surface profiler (Tencor Instruments). The electrical properties of the interconnection lines were examined with a semiconductor parameter analyzer (Agilent 4155C) in air.

3. Results and Discussion

The TEM image (a), XRD pattern (b), and absorption spectrum (c) taken from the Ag NPs synthesized in this work are presented in Fig. 1; their selected area electron diffraction (SAED) pattern is shown in the inset of Fig. 1(a). The TEM image demonstrates the dispersed Ag NPs with average diameters of 20 nm, and the spots shown in the SEAD pattern reveal that the Ag NPs are crystalline. The XRD pattern taken from the powder of Ag NPs shows that the peak positions match well with the standard data of

*E-mail address: sangsig@korea.ac.kr

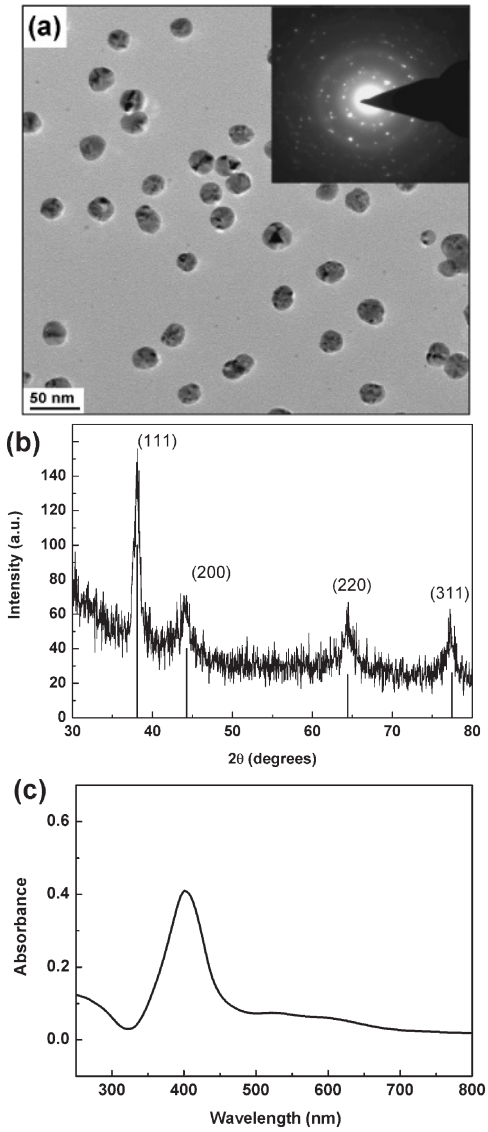

Fig. 1. TEM image (a), XRD pattern (b), and absorption spectrum (c) taken from the Ag NPs. Their SAED pattern is shown in the inset of (a).

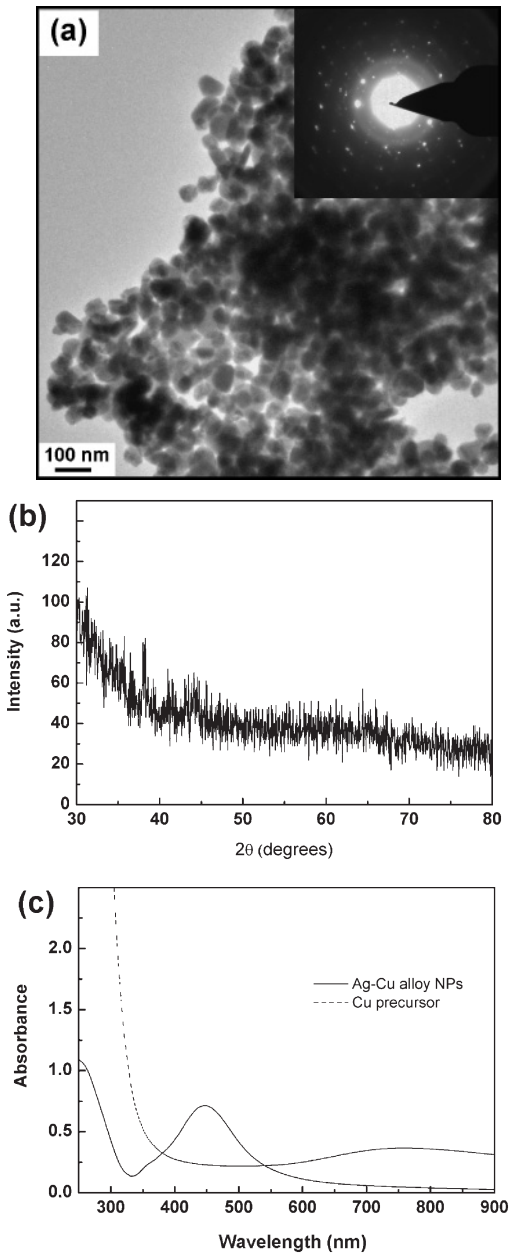

Fig. 2. TEM image (a), XRD pattern (b), and absorption spectrum (c) taken from the Ag–Cu alloy NPs. Their SAED pattern is shown in the inset of (a).

JCPDS file 04-0783, revealing that the synthesized NPs are indeed Ag ones. In addition, a broad band is present at around 400 nm in the absorption spectrum taken from the Ag NPs dispersed in water, which originates from the plasmon resonances in the Ag NPs.

The TEM image (a), XRD pattern (b), and absorption spectrum (c) taken from the Ag–Cu alloy NPs prepared in this study are presented in Fig. 2; their SAED pattern is shown in the inset of Fig. 2(a). The TEM image reveals that the average size of the Ag–Cu alloy NPs is 50 nm; their size is 2.5 times larger than that of the Ag NPs. In contrast to the Ag NPs, no peaks are seen in the XRD pattern of the Ag–Cu alloy NPs. Nevertheless, spots are seen in the SAED pattern obtained from the latter. The presence of these spots, as observed for the Ag NPs, indicates that the Ag–Cu alloy NPs are not amorphous but crystalline and X-ray peaks should therefore be present in their XRD pattern. One of the reasons for the absence of X-ray peaks is that their X-ray cross-section coefficient is much lower than that of the Ag NPs, due to their alloy characteristics. The formation of the Ag–Cu alloy NPs was additionally confirmed by absorption spectroscopy. In the absorption spectra shown in Fig. 2(c), the absorption band observed for the Cu precursor solution peaks at 750 nm, whereas a single peak is present at 450 nm for the Ag–Cu alloy NPs dispersed in water. This peak position is different from that of the Ag NPs. In addition, energy dispersive X-ray spectroscopy (EDS) was used to confirm the presence of Cu ions in the alloy NPs.

An optical microscope image taken for a representative interconnection line made of NPs fabricated on a PES substrate is shown in Fig. 3. Two different interconnection lines were fabricated on separate PES substrates. One was composed of Ag NPs and the other of Ag–Cu alloy NPs. The thicknesses of the interconnection lines made of the Ag NPs and Ag–Cu alloy NPs were about 300 and 270 nm, respectively. These lines are hereafter referred to as the Ag NP line and the Ag–Cu NP line, respectively.

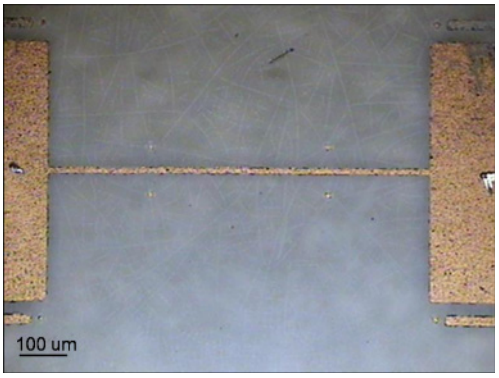

Fig. 3. (Color online) Optical microscope image of a patterned Ag NP line.

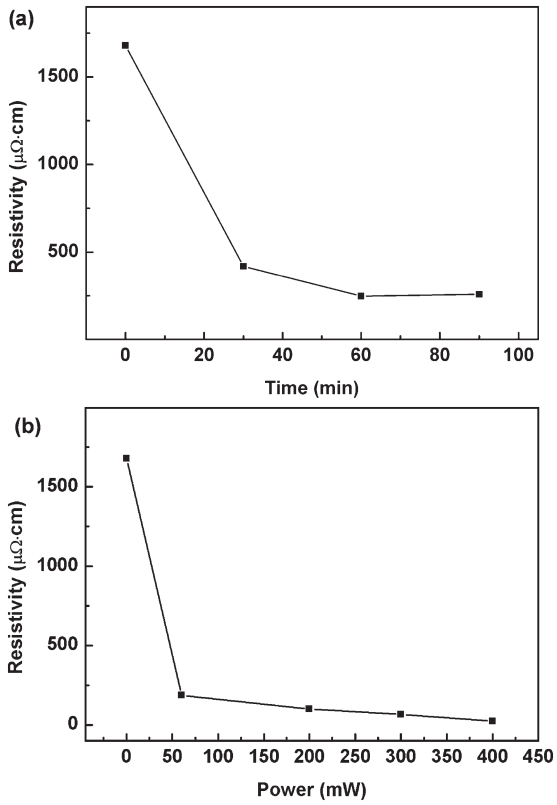

Fig. 4. The resistivity of the Ag NP line plotted as a function of (a) the irradiation time at a fixed laser power of 60 mW and (b) the laser power for a fixed irradiation time of 30 min.

The resistivity of the Ag NP line patterned on the PES substrate was measured as functions of the irradiation time and power. The resistivity of the line is estimated from the following equation:

$$\rho = R \cdot A/L, \tag{1}$$

where R is the resistance obtained from the slope of the current–voltage (I–V) curves, A is the cross-section area and L is the length of the line. The width and length of the patterned interconnection lines are 15 and 800 μm, respectively. The resistivity of the Ag NP line is plotted in Fig. 4(a) as a function of the irradiation time of the 488-nm wavelength light; the power of the light irradiated on the Ag line was 60 mW. The resistivity of the Ag line decreased as

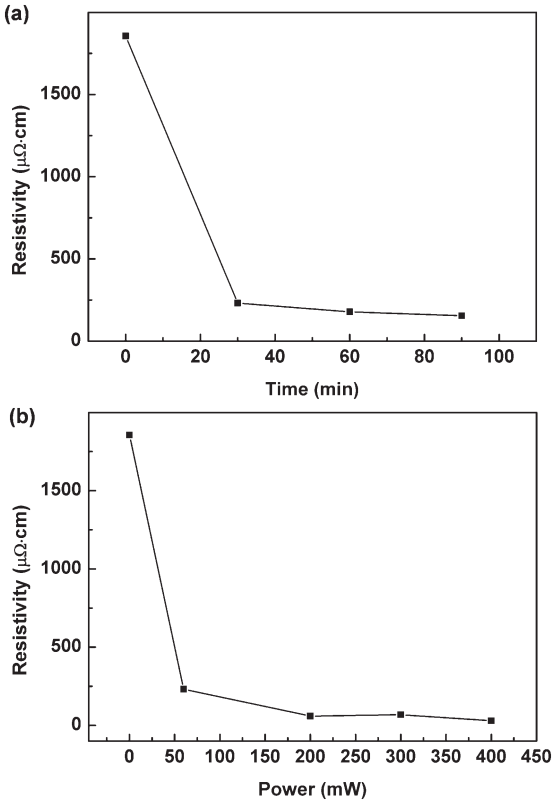

Fig. 5. The resistivity of the Ag–Cu alloy NP line plotted as a function of (a) the irradiation time at a fixed laser power of 60 mW and (b) the laser power for a fixed irradiation time of 30 min.

the irradiation time increased. For an irradiation time of 90 min, the resistivity was reduced from 1800 to 200 μΩ·cm. The resistivity of the Ag NP line is plotted in Fig. 4(b) as a function of the power of the light. As the irradiation power increased from 0 to 400 mW, the resistivity of the Ag line decreased from 1800 to 25 μΩ·cm; the irradiation time was fixed at 30 min for the measurement of the resistivity. Furthermore, for the Ag–Cu alloy NP line, the dependence of the resistivity on the irradiation time and power was examined. The resistivity is plotted in Fig. 5 as functions of the irradiation time and power. When the light was irradiated on the Ag–Cu alloy NP line for 90 min, its resistivity was reduced from 1800 to 140 μΩ·cm. The resistivity of the Ag–Cu alloy NP line decreased from 1800 to 30 μΩ·cm as the power of the light was increased from 60 to 400 mW. The observation described above reveals that the dependence of the electrical characteristics of the Ag NP and Ag–Cu alloy NP lines on the irradiation time and power are nearly the same.

Figure 6 shows the SEM images taken from the four different lines made of the as-synthesized Ag NPs (a), irradiated Ag NPs (b), as-synthesized Ag–Cu alloy NPs (c), and irradiated Ag–Cu alloy NPs (d). The lines made of the irradiated NPs were obtained by irradiating the lines made of the as-synthesized NPs with light with a power of 400 mW for 30 min. A careful comparison made between the SEM images reveals that the irradiated NPs are larger in size than the as-synthesized NPs. Note that the average sizes of the as-synthesized and irradiated Ag NPs and of the as-synthesized and irradiated Ag–Cu alloy NPs obtained from the SEM images are 20, 80, 50, and 73 nm, respectively. This

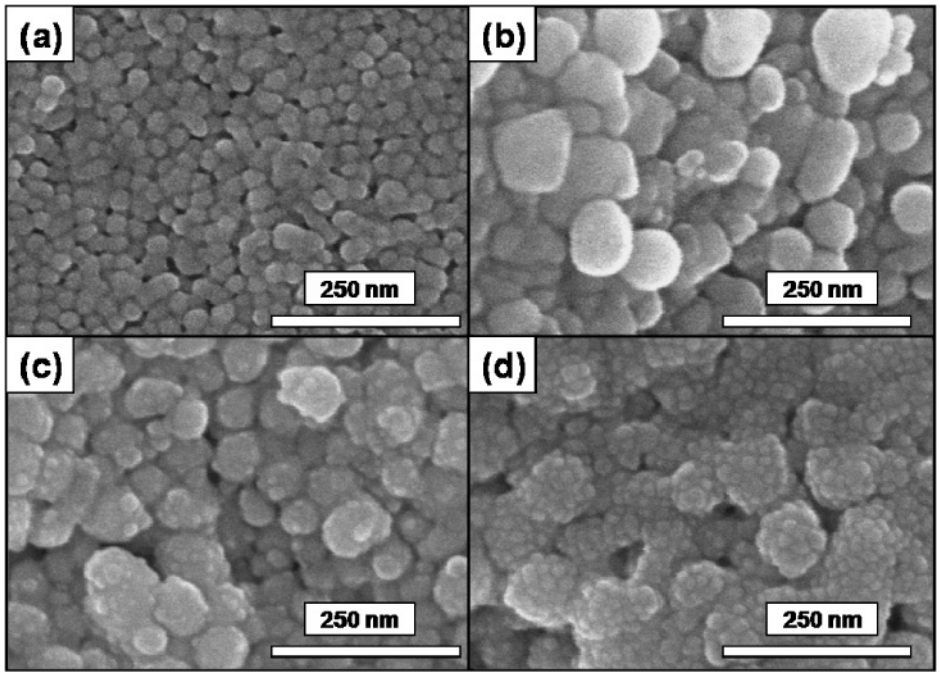

Fig. 6. SEM images taken from the four different lines made of the as-synthesized Ag NPs (a), irradiated Ag NPs (b), as-synthesized Ag–Cu alloy NPs (c), and irradiated Ag–Cu alloy NPs (d).

observation indicates that the optical heating leads to the sintering of the NPs. The sintering process causes both an increase in the size of the NPs and necking between them. The increase in the size of the Ag NPs is more significant than that of the Ag–Cu alloy NPs, but the necking phenomenon is more remarkable for the Ag–Cu alloy NPs than for the Ag NPs.

In the case of the films consisting of metal NPs, the resistivity of the films is related to the size of the NPs, the thickness of the films and the reflection coefficient in the interfaces between the NP grains. The dependence of the resistivity on the size of NPs and on the thickness of the films increases when the size of the NPs and the thickness of the films are smaller than the mean free path of electrons in the corresponding metal bulk. Also, the reflection coefficients of the interfaces between the NP grains are determined by the grain boundary condition of the NPs and by the insulating materials barriers present between the NP grains. Therefore, the total resistivity of the films is considered to be the sum of the bulk resistivity and the additional resistivity due to the effects of the grain boundaries.[14,15] As described in refs. 14 and 15, the total resistivity ρ_F of metallic films is expressed as

$$\rho_F \cong \rho_g + \rho_s \quad K \gg 1, \tag{2}$$

where ρ_g is the grain-boundary resistivity, ρ_s is the resistivity depending on external surface scattering and K is the ratio of the film thickness t to the mean free path l_0. Under the Mayadas–Shatzkes and Fuchs–Sondheimer models, eq. (2) can be expressed as

$$\rho_F \cong \frac{\rho_0}{1 - \frac{3}{2}\alpha + 3\alpha^2 - 3\alpha^3 \ln\left(1 + \frac{1}{\alpha}\right)} + \rho_0 l_0 \frac{3}{8}\left(\frac{1-p}{t}\right), \tag{3}$$

where ρ_0 is the background resistivity and p is the fraction of electrons scattered at the external surfaces. Note that p is zero for randomly oriented NP grains and α is defined in eq. (3) as

$$\alpha = \frac{l_0}{a}\frac{r}{1-r}, \tag{4}$$

where a is the grain diameter (or the average size of the NPs) and r is the reflection coefficient at the grain-boundary of the NP grains. These models can be applied to explain the results shown in Figs. 4 and 5. Note that, for the line composed of Ag NPs, ρ_0 is 1.63 μΩ·cm,[14,15] and for the line composed of Ag–Cu alloy NPs, ρ_0 is 4 μΩ·cm.[16] And for both of the lines, the mean free path l_0 was used in this study.[14,15] The decreases in the resistivities are attributed to the increase in both the NP grain size and the reflection coefficient. Our estimation performed under the models reveals the reflection coefficient of the line composed of Ag NPs estimated by eq. (3) is reduced from 0.998 to 0.969 when the as-deposited film was irradiated by a laser power of 400 W for 30 min. Similarly, the estimated reflection coefficient of the line composed of Ag–Cu alloy NPs is reduced from 0.998 to 0.947 when the as-deposited film was irradiated under the same conditions. The reflection coefficient of the irradiated Ag–Cu alloy NPs is lower than that of the irradiated Ag NPs. This estimated result is consistent with the observation that the necking phenomenon is more remarkable for the Ag–Cu alloy NPs than for the Ag NPs. Therefore, one of the main reasons for the decrease in the reflection coefficient is the necking phenomenon of the metal NPs induced by the laser heating.

In addition to the decrease in the reflection coefficient of the metal NPs, the removal of the PVP present on the surfaces of the NPs by the optical heating can also contribute

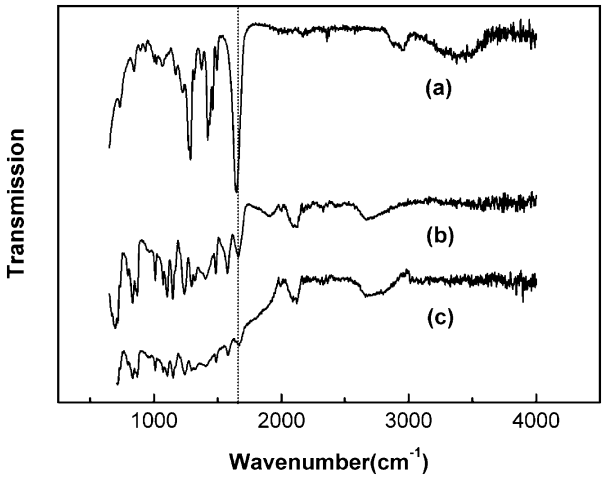

Fig. 7. FTIR spectra taken from the PVP material itself (a) and the Ag NP lines before (b) and after (c) the laser heating. The peaks associated with the PVP material are marked by a dotted line in the spectra.

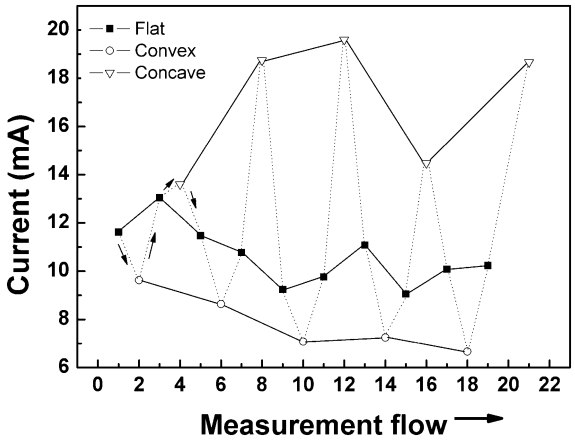

Fig. 8. The current measured at a bias voltage of 1 V for the Ag–Cu alloy NP lines on convex, flat, or concave substrates. The dotted line indicates the sequential order of the measurement.

to the decrease in the resistivity of the laser-heated metal lines. We attempted to wash out the PVP utilized in the synthesis of the metal NPs with acetone and methanol prior to the patterning of the metal lines made of NPs. Nevertheless, the presence of PVP material in the metal line was observed by Fourier transform infrared (FTIR) spectroscopy. The FTIR spectra taken from the PVP material itself and from the as-synthesized and irradiated lines composed of NPs are plotted in Fig. 7. In these FTIR spectra, the peak associated with PVP is present at 1640 cm^{-1}, indicating that PVP is still present in the NPs, even though they were washed in order to remove it: the peak is marked by a dotted line in the spectra. The presence of PVP in the NPs degrades their conductance, since it is an insulating material. Furthermore, the FTIR spectra demonstrate that the intensity of the PVP-related peak is weakened after the optical heating of the NPs. This weakening is due to the evaporation of PVP caused by the optical heating. The removal of the insulating PVP material from the NPs enhances their conductance. Therefore, the reduction of the estimated reflection coefficient of the line composed of NPs is caused not only by the necking of the NPs, but also by the removal of the insulating PVP material present in them.

Furthermore, the bending effect on the current flowing in the Ag–Cu alloy NP line was investigated. Figure 8 shows the effect of cyclic bending on the current in the Ag–Cu alloy NP line. The current was measured at a bias voltage of 1 V for the NP lines on convex, flat, or concave substrates. In Fig. 8, the dotted line indicates the sequential order of the measurement. The three solid lines classify the magnitudes of the currents measured for the NP line under the convex, flat and concave conditions. The variation in the magnitude of the current is due to the change in the reflection coefficient in the grain boundary condition of the metal NPs according to the bending of the NP line. Compared with the flat NP line, the current is decreased in magnitude by about 25% for the NP line under the convex condition, due to the increased separation between the NP grains. The magnitude of the current is increased by about 54% for the NP line under the concave condition. The increased magnitude of the current is due to the reduction of the separation between the NP grains. Because these variations of the separation between grains induced the changes of the reflection coefficient, not the size of the NPs, the resistivities are affected by the bending conditions of the substrate. As the number of measurements increases, the magnitude of the current decreases by 20–30% for the flat NP line and for the NP line under the convex condition, while it increases for the NP line under the concave condition. This observation illustrates the potential for using metal NP lines as the metal electrodes and lines in flexible electronics subjected to bending.

4. Conclusions

In this work, Ag NPs and Ag–Cu alloy NPs were synthesized by the polyol method. Interconnection lines made of the Ag and Ag–Cu alloy NPs patterned on PES substrates were heated optically with 488-nm wavelength light. When the light was irradiated on the metal NP lines, their resistivities were reduced dramatically because both the increased size and the decreased reflection coefficient cause the reduction of electron scattering between the metal NPs. The decrease in the reflection coefficient is related to both the necking of the NPs and the elimination of PVP in the lines caused by the optical heating. The dependences of the electrical characteristics of the Ag NP and Ag–Cu alloy NP lines on the irradiation time and power were nearly the same. In addition, the current decreased for the metal NP line under the convex condition, whereas it increased under the concave condition, as compared with the flat condition. The variation of the current is due to the significant change in the reflection coefficient of the grain boundary of the NPs caused by the change in the separation between the metal NPs.

Acknowledgements

This work was supported by the Industrial-Educational Cooperation Program between Korea University and LG. Philips LCD, the National R&D Project for Nano Science and Technology (10022916-2006-22), the Center for Integrated-Nano-Systems (CINS) of the Korea Research Foundation (KRF-2006-005-J03601), the "SystemIC2010"

project of the Korea Ministry of Commerce, Industry and Energy, the Korea Science and Engineering Foundation (KOSEF) through the National Research Lab. Program [R0A-2005-000-10045-02 (2007)], and the Nano R&D Program (M10703000980-07M0300-98010).

1) D. Kim, S. Jeong, B. K. Park, and J. Moon: Appl. Phys. Lett. **89** (2006) 264101.
2) J. W. Park and S. G. Baek: Scr. Mater. **55** (2006) 1139.
3) H. H. Lee, K. S. Chou, and K. C. Huang: Nanotechnology **16** (2005) 2436.
4) A. Kamyshny, M. Ben-Moshe, S. Aviezer, and S. Magdassi: Macromol. Rapid Commun. **26** (2005) 281.
5) B. K. Park, D. Kim, S. Jeong, J. Moon, and J. S. Kim: Thin Solid Films **515** (2007) 7706.
6) T. Y. Choi, D. Poulikakos, and C. P. Grigoropoulos: Appl. Phys. Lett. **85** (2004) 13.
7) S. H. Ko, H. Pan, C. P. Grigoropoulos, C. K. Luscombe, J. M. J. Frechet, and D. Poulokakos: Appl. Phys. Lett. **90** (2007) 141103.
8) K. Barmak, C. Cabral, K. P. Rodbell, and J. M. E. Harper: J. Vac. Sci. Technol. B **24** (2006) 2485.
9) H. Han, Y. Zoo, J. W. Mayer, and T. L. Alford: J. Appl. Phys. **102** (2007) 36101.
10) Y. Zhao, J.-J. Zhu, J.-M. Hong, N. Bian, and H.-Y. Chen: Eur. J. Inorg. Chem. (2004) 4072.
11) B. K. Park, S. Jeong, D. Kim, J. Moon, S. Lim, and J. S. Kim: J. Colloid Interface Sci. **311** (2007) 417.
12) A. Slistan-Grijalva, R. Herrera-Urbina, J. F. Rivas-Silva, M. Avalos-Borja, F. F. Castillon-Barraza, and A. Posada-Amarillas: Physica E **25** (2005) 438.
13) H. Jiang, K. S. Moon, and C. P. Wong: Proc. IEEE Int. Conf. Advanced Packaging Materials: Process, Properties and Interface, 2005, p. 173.
14) C. R. Pichard, C. R. Tellier, and A. J. Tosser: J. Phys. D **12** (1979) L101.
15) E. I. Tochitskii and N. M. Belyavskii: Phys. Status Solidi A **61** (1980) K21.
16) B. Zhao, H. Kimand, and Y. Shimogaki: Jpn. J. Appl. Phys. **44** (2005) L1278.